Signal Transformed Internal Model Control for Non-raster Scanning of Piezo-actuated Nanopositioning Stages

Jie Ling, Zhao Feng, Min Ming, Zhao Guo, and Xiaohui Xiao*

International Journal of Control, Automation and Systems 18(8) (2020) 1915-1925

ISSN:1598-6446 (print version)
eISSN:2005-4092 (electronic version)

To link to this article:
http://dx.doi.org/10.1007/s12555-019-0064-y

International Journal of Control, Automation and Systems 18(8) (2020) 1915-1925
http://dx.doi.org/10.1007/s12555-019-0064-y
ISSN:1598-6446 eISSN:2005-4092
http://www.springer.com/12555

Signal Transformed Internal Model Control for Non-raster Scanning of Piezo-actuated Nanopositioning Stages

Jie Ling, Zhao Feng, Min Ming, Zhao Guo, and Xiaohui Xiao*

Abstract: This paper proposes a new signal transformed internal model control (STIMC) scheme for non-raster scanning patterns of piezo-actuated nanopositioning stages. To smooth the scanning signals superimposed with a ramp or time-varying amplitudes, a signal transformation operator is calculated to convert the references into standard harmonic waveforms. An inverse transformation operator is then added in the control loop to generate the driving signals. For the contained internal model control (IMC) design, an H_∞ mixed-sensitivity method is utilized for the first order internal mode synthesis. A second and a third internal modes are included in the IMC for alleviating residual high-frequency errors resulted from the nonlinearity of hysteresis. To verify the proposed STIMC scheme, comparative experiments with conventional IMC are conducted based on a nanopositioning platform. Results prove that the STIMC is effective on non-raster signals' tracking. A same tracking precision for Lissajous scanning can be obtained by STIMC compared with IMC. An improvement of larger than 50% and 80% of root-mean-square errors can be obtained for cycloid and spiral scanning patterns, respectively.

Keywords: Internal model control, nanopositioning stage, non-raster scanning, signal transformed method.

1. INTRODUCTION

Piezo-actuated flexure stages are widely utilized as vital components to perform high-speed high-precision positioning tasks in the devices of scanning probe microscopes (SPMs) [1, 2]. For imaging of specimens in SPMs, nanopositioning stages are usually driven as a scanner in a raster pattern [3]. The raster scanning mode is operated by actuating the x-axis with a triangular signal and the y-axis with a ramp or staircase signal [4, 5]. The dominating advantage of the raster scanning mode lies in simple image reconstruction results from constant velocity and uniform sampling data in a square grid [1, 6]. However, due to the inherent resonant nature of the nanopositoning stages, the high-order harmonics contained in input triangular signals may excite the lightly damped modes and lead to undesirable vibration as well as loss of positioning accuracy [7]. For this, the scanning bandwidth of raster pattern is restricted lower than $1/100 - 1/10$ of the nanopositioner's first resonant frequency [8].

For the past decades, a number of high-bandwidth nanopositioning stages are designed for high-speed raster scanning [9–11]. However, with the increase of first resonant frequency, the travel stroke of a nanopositioner is generally decreased [10]. Herein, abundant feedforward [12,13] and feedback control approaches [2,5,7–10,14,15] have been reported to compensate for scan-induced vibration errors or to damp the vibrational modes, and hence to improve tracking performance for high-speed raster scanning.

Recently, an alternative approach to significantly speed up the scanning motions of nanopositioners is utilizing non-raster patterns including Lissajous, cycloid and spiral scanning signals [1, 6]. All the three non-raster patterns track sinusoidal or cosinoidal reference signals in the lateral xy plane of the nanopositioning stage [16–19]. A specific non-raster pattern can be chosen according to the scanning specifications (i.e., bandwidth, resolution, scanning rate, and sampling frequency, etc.) as well as the ease of imaging reconstruction. Unlike raster signals, all the three non-raster signals are generated based on harmonic waveforms, of which the frequency spectrums are much narrower. Hence, on the one hand, the primary advantage of non-raster pattern is a much faster scanning rate than raster pattern providing a limited bandwidth of a nanopositioning stage [16]. On the other hand, the tracking performance can be remarkably improved by feedback control loops with limited closed-loop bandwidth as external

Manuscript received January 26, 2019; revised May 27, 2019 and October 12, 2019; accepted November 18, 2019. Recommended by Associate Editor Vu Nguyen under the direction of Editor Won-jong Kim. This work was supported by the Project funded by China Postdoctoral Science Foundation under Grant No. 2018M642907, Shenzhen Science and Technology Program under Grant No. JCYJ20170306171514468 and Natural Science Foundation of China under Grant No. 51375349.

Jie Ling, Zhao Feng, Min Ming, Zhao Guo, and Xiaohui Xiao are with School of Power and Mechanical Engineering, Wuhan University, 430072, Wuhan, China. (e-mails: {jamesling, fengzhaozhao7, mingnmin_whu, guozhao, xhxiao}@whu.edu.cn). Xiaohui Xiao is also with Shenzhen Institute of Wuhan University, Shenzhen 518057, China.
* Corresponding author.

noise or disturbance can be attenuated [19]. However, control methods for raster patterns are not always applicable for non-raster applications because of the aforementioned differences.

Regarding the precise tracking of harmonic signals with constant amplitudes, internal model control (IMC) is an effective approach for asymptotically obtaining zero tracking errors while rejecting deterministic disturbances and external noise simultaneously with a relatively low control bandwidth [20]. Applications of IMC for non-raster trajectories' tracking are well reported in some works [16–21]. Conventional IMC integrated with higher order harmonics of the sinusoids was developed for high-speed Lissajous tracking in [20]. This work was extended into video-rate Lissajous scanning by adding integral resonant controller into an IMC scheme in [16]. A novel controller cooperating IMC with a proportional-integral term was also designed and tuned for video-rate cycloid scanning in [17]. Different from the above two trajectories, the time-varying amplitudes of a spiral reference will lead to proportional tracking errors during scanning, which makes it harder to track. A minimal-order IMC was presented for high-speed spiral scanning in [18]. Subsequently, significant control performance improvements could be achieved by combining a novel amplitude modulating waveform with IMC for spiral trajectory, which was introduced in [21] for video-rate spiral scanning of SPMs. The above efforts have made notable progress for non-raster scanning patterns. However, for some occasions where scanning patterns need to be switched, control schemes need to be changed correspondingly. Each of the aforementioned IMC approaches is specific for a certain non-raster signal. Moreover, it is difficult to directly apply the IMC approach in [21] for the spiral trajectory into a Lissajous trajectory tracking. Conversely, the IMC combined with damping control in [16] is not suitable for tracking of spiral trajectory with varying amplitudes. Therefore, a uniform IMC scheme for all the three non-raster patterns needs to be investigated.

For this, the motivation of this paper is to develop a uniform IMC scheme for the three non-raster patterns. Inspired by the reported signal transformation approach (STA) for high-speed raster scanning of nanopositioning stages in [22], the similar characteristic of a harmonic waveform superimposed upon another signal among the three non-raster patterns can be considered in the IMC design. A signal transformed internal model control (STIMC) is proposed in this work. The Lissajous, cycloid and spiral scanning signals are transformed into standard harmonic formats (sinusoidal or cosinoidal waveform) with fixed amplitude before entering the feedback control loop. A set of multi-mode internal model controllers are then designed and tuned for the transformed reference's tracking. Referred to [16], a second and a third harmonics of the transformed reference are contained in the IMC to compensate for the residual tracking errors resulted from the nonlinearity of hysteresis. An inverse transformation of the generated control signals is operated before driving the nanopositioning stage. Compared with the conventional IMC scheme, the proposed STIMC is effective for tracking of harmonic references with time-varying amplitudes. The main contribution of this paper is two-fold. Firstly, the uniform IMC scheme is introduced for the three non-raster scanning patterns. The signal transformations as well as the inverse transformations are presented in this work. Secondly, a set of comparative experiments of the STIMC versus conventional IMC on a nanopositioning stage are conducted to demonstrate the superiority of the proposed STIMC.

The reminder of this paper is arranged as follows: Experimental system and its identification are described in Section 2. In Section 3, the proposed STIMC is discussed. The signal transformations as well as the inverse transformations of Lissajous, cycloid and spiral scanning signals are analyzed. Section 4 presents the control design and the experimental implementation. Finally, conclusion and future work are drawn in Section 5.

2. SYSTEM DESCRIPTION

2.1. Experimental setup

The physical experiment system employed in this paper is depicted in Fig. 1. A commercial product of a three-axis piezo-actuated nanopositioning stage (model: P-561.3CD, from Physik Instrumente Co., Ltd.) is utilized in this work for the verification of the proposed STIMC.

The signal flow of the control loop is shown in Fig. 1(b). For each axis, the control input voltage with a range of 0-10 V is produced by 16-bit digital to analog interfaces (DACs) of the data output module in real-time controller (model: MicroLabBox, from dSPACE Co., Ltd.). A piezo amplifier module (model: E-503.00, from Physik Instrumente Co., Ltd.) with a fixed gain of 10 amplifies the input voltage and generates excitation voltage between 0 to 100 V. The output of each motion axis with a stoke of 100 μm, which is read by a PZT servo submodule (model: E-509.C3A, from Physik Instrumente Co., Ltd.), is subsequently passed to the data input module in dSPACE MicroLabBox with 16-bit analog to digital interfaces (ADCs).

The controller is designed in MATLAB®/Simulink block diagram on the host PC (running on Windows 10 and an Intel Core i5-8300H CPU, where the Solver is chosen as fixed-step ode 4 with a step size being 0.1 ms and the other settings being defaults.), and then downloaded and executed on the target dSPACE MicroLabBox in the real-time software environment of dSPACE ControlDesk.

In this work, only the x-axis and y-axis in the lateral were used to implement the proposed STIMC for a two-input-two-output (TITO) scanning system and the sam-

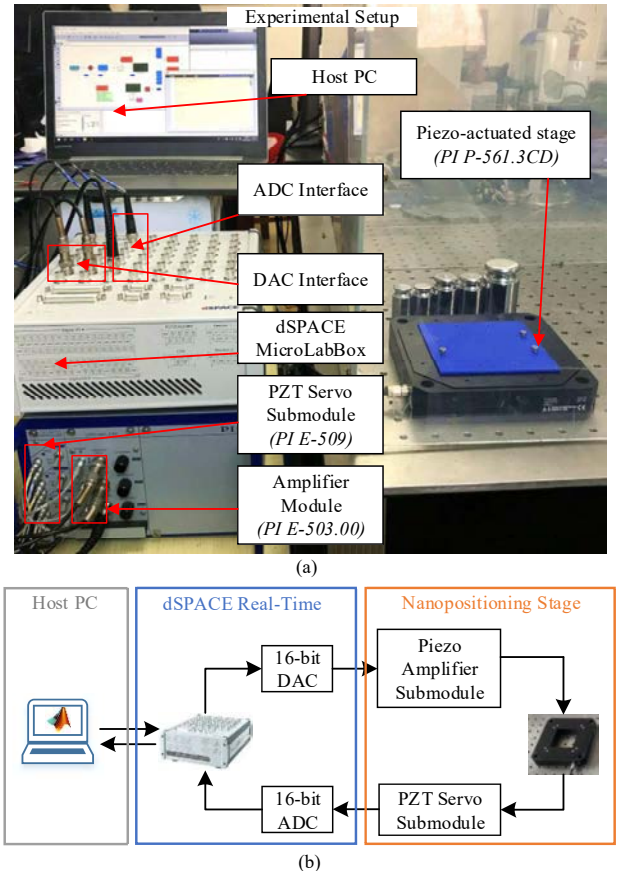

Fig. 1. The experimental setup of a piezo-actuated nanopositioning system: (a) experimental platform; (b) block diagram of signal flow.

pling frequency of the control loop was set as 10 kHz.

2.2. System identification

A chirp signal with a constant amplitude at 200 mV from $0 \sim 500$ Hz was fed into the x and y axes. A low magnitude of input voltage was used here to avoid distortion from hysteresis. Frequency responses are recorded by a spectrum analyzer as presented in Fig. 2 (in dashed blue line). Time domain outputs of the displacements are recorded by the data input module in dSPACE. A linear time invariant (LTI) models from the input voltage to the output displacement of the axes are then obtained using the Identification Toolbox of MATLAB, which can be shown as:

$$G_{xx}(s)=\frac{\begin{array}{c}92.83s^4-2.506\times10^5s^3+5.589\times10^8s^2\\-2.434\times10^{11}s+5.213\times10^{14}\end{array}}{\begin{array}{c}s^5+1347s^4+3.209\times10^6s^3\\+2.654\times10^9s^2+2.468\times10^{12}s\\+7.611\times10^{14}\end{array}}, \tag{1}$$

$$G_{xy}(s)=\frac{\begin{array}{c}7.865s^4-1.311\times10^4s^3+1.829\times10^7s^2\\-2.011\times10^{10}s-1.312\times10^{12}\end{array}}{\begin{array}{c}s^5+417.3s^4+3.342\times10^6s^3\\+1.102\times10^9s^2+2.851\times10^{12}s\\+6.639\times10^{14}\end{array}}, \tag{2}$$

$$G_{yx}(s)=\frac{\begin{array}{c}7.884s^4-1.302\times10^4s^3+1.833\times10^7s^2\\-2.009\times10^{10}s-1.313\times10^{12}\end{array}}{\begin{array}{c}s^5+411.4s^4+3.375\times10^6s^3\\+1.095\times10^9s^2+2.842\times10^{12}s\\+6.642\times10^{14}\end{array}}, \tag{3}$$

$$G_{yy}(s)=\frac{\begin{array}{c}89.7s^4-2.478\times10^5s^3+5.328\times10^8s^2\\-2.388\times10^{11}s+4.955\times10^{14}\end{array}}{\begin{array}{c}s^5+1347s^4+3.242\times10^6s^3\\+2.666\times10^9s^2+2.514\times10^{12}s\\+7.333\times10^{14}\end{array}}, \tag{4}$$

where G_{xy} stands for transfer function from the input voltage $[V]$ of $x-$axis to the output displacement $[\mu m]$ of $y-$axis, and so forth.

The comparative bode diagrams of the identified model and measured data are displayed in Fig. 2. From (1)-(4) and Fig. 2, it can be clearly found that the frequency responses of x and y axis are similar with the same first resonant frequency of 210 Hz. The cross-coupling of this stage is well attenuated at low frequencies with a magnitude less than -40 dB in the range of $1\sim100$ Hz. Hence, in this paper, the cross-coupling effect is not considered in the controller design. Taking into account that the dynamics of

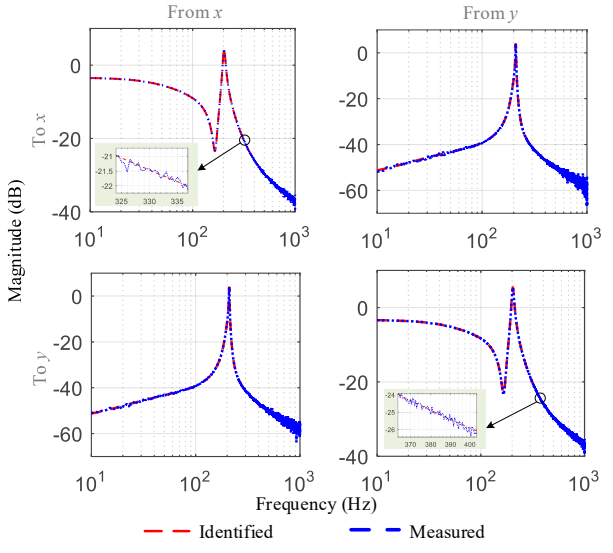

Fig. 2. Comparative bode digrams of the identified model and measured data.

the dominate x and y axes are nearly the same, the IMC controllers for the two axes are designed with the same parameters in the following sections.

Remark 1: In this paper, we aim to design a controller for scanning of a nanopositioning stage. However, the proposed control scheme can also be applicable for a robotic system or a machine tool system where non-raster motions or some specific repetitive tasks are required.

3. PROPOSED CONTROL SCHEME

In this section, the signal transformation operations for three types of non-raster signals are discussed in advance before controller design. Then, the STIMC scheme is proposed, followed by the stability as well as the performance analysis in details.

3.1. Signals transformation

3.1.1 Lissajous scanning

The Lissajous scanning pattern involves multi-resolution imaging. As shown in Fig. 3(a), a Lissajous scanning pattern consists of constant amplitudes and constant frequencies in an xy scanning plane. It can be achieved by applying the following signals into x and y axes of the nanopositioning stage:

$$x(t) = A_x \cdot \cos(2\pi f_x t), \tag{5}$$
$$y(t) = A_y \cdot \cos(2\pi f_y t), \tag{6}$$

where A_x and A_y are positive constants denoting the scanning amplitudes of x and y axes. The scanning rates f_x and f_y fulfill a relationship which can be cauculated as

$$\frac{f_x}{f_y} = \frac{2M}{2M-1}, \tag{7}$$

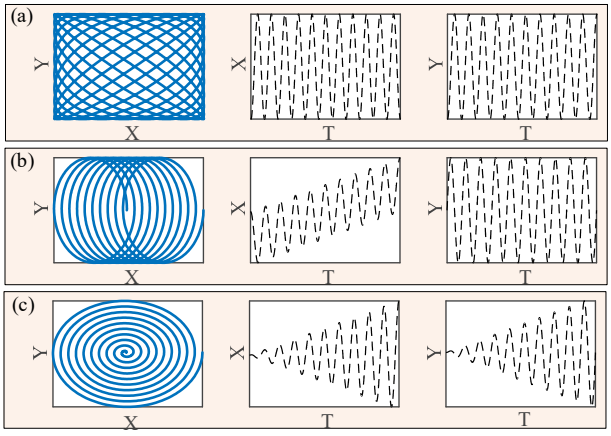

Fig. 3. Scanning patterns of the three types of non-raster signals. (a) Spiral scanning; (b) Cycloid scanning; (c) Lissajous scanning.

where M is a positive constant related to the scanning resolution.

It can be seen that both the two axes of Lissajous scanning pattern are standard cosinoidal waveforms. A conventional IMC therefore can be applied directly for tracking control. To maintain the consistent form in the STIMC and to obtain unit amplifications, the operators $\Phi_{ST}(s)$ and $\Phi_{IST}(s)$ for the two axes are chosen as,

$$\Phi^{liss}_{ST_x}(t) = 1/A_x, \;\; \Phi^{liss}_{ST_y}(t) = 1/A_y, \tag{8}$$
$$\Phi^{liss}_{IST_x}(t) = A_x, \;\; \Phi^{liss}_{IST_y}(t) = A_y. \tag{9}$$

3.1.2 Cycloid scanning

The two adjacent scan lines in a cycloid scanning pattern can remain fixed during the scanning process, such that the resolution is consistent throughout the scanned area (see Fig. 3(b)). In addition, it is reported that a cycloid scanning pattern can reduce the scan time considerably by focusing the scanning on a specific sample rather than the whole scanned area [17]. This pattern can be implemented through driving the axes by:

$$x(t) = \alpha \cdot t + \beta \cdot \cos(2\pi f_{cyc} t), \tag{10}$$
$$y(t) = \beta \cdot \sin(2\pi f_{cyc} t), \tag{11}$$

where the scanning rate f_{cyc} is chosen for both x and y axes. α is a constant representing the slope of the ramp signal. β stands for scanning amplitude.

In this pattern, the transformation operators are selected as

$$\Phi^{cyc}_{ST_x}(t) = \frac{x(t) - \alpha \cdot t}{\beta \cdot x(t)}, \;\; \Phi^{cyc}_{ST_y}(t) = 1/\beta, \tag{12}$$
$$\Phi^{cyc}_{IST_x}(t) = \beta + \frac{\alpha \cdot t}{\widetilde{u}_x(t)}, \;\; \Phi^{cyc}_{IST_y}(t) = \beta. \tag{13}$$

3.1.3 Spiral scanning

Compared to the above two patterns, the spiral scanning pattern can provide a uniform image resolution at each point of the scanned area without retracing any part of the targeted area [22]. In this pattern as shown Fig. 3(c), the x and y axes are actuated by the following signals as

$$x(t) = r(t) \cdot \cos(2\pi f_{spi} t), \tag{14}$$
$$y(t) = r(t) \cdot \sin(2\pi f_{spi} t), \tag{15}$$

where f_{spi} is the scanning rate of the two axes. $r(t) = p \cdot f_{spi} \cdot t$ is the time-varying amplitude with the pitch p defined as

$$p = \frac{Spiral\ radius \times 2}{Number\ of\ curves - 1}. \tag{16}$$

The transformation operators for the spiral pattern can be calculated as,

$$\Phi^{spi}_{ST_x}(t) = \Phi^{spi}_{ST_y}(t) = \frac{1}{p \cdot f_{spi} \cdot t}, \tag{17}$$
$$\Phi^{spi}_{IST_x}(t) = \Phi^{spi}_{IST_y}(t) = p \cdot f_{spi} \cdot t. \tag{18}$$

3.2. STIMC scheme

The object of STIMC is to track the three non-raster scanning signals using a uniform IMC scheme. For this, the reference trajectories of each axis is transformed through operator $\Phi_{ST}(s)$ into standard sinusoidal or cosinoidal waveforms such that an IMC controller can be designed for tracking of the harmonic waveforms with a fixed frequency.

The following content describes the IMC design. Taking an example of the control design for x-axis, the proposed STIMC scheme is shown in Fig. 4. A multi-mode IMC is applied for tracking of the transformed reference $\widetilde{r}_x$. An integral controller C_0 is included for the fast convergence of errors. A first order harmonic internal mode of the tracked reference is used to obtain precise tracking of the input sinusoidal or cosinoidal waveform with a fixed fundamental frequency. In view of the nonlinearity of hysteresis [23], residual tracking errors resulted from the infinite number of harmonics in addition to the reference's fundamental component will deteriorate the tracking performance [16]. In Fig. 4, the components of the IMC are designed as,

$$C_0(s) = \frac{K_i}{s}, \tag{19}$$

$$C_1(s) = \frac{a_1 s + b_1}{1 + s^2/\omega_1^2} = \frac{a_1 s + b_1}{1 + s^2/(2\pi f_x)^2}, \tag{20}$$

$$C_2(s) = \frac{a_2 s + b_2}{1 + s^2/\omega_2^2} = \frac{a_2 s + b_2}{1 + s^2/(2 \times 2\pi f_x)^2}, \tag{21}$$

$$C_3(s) = \frac{a_3 s + b_3}{1 + s^2/\omega_3^2} = \frac{a_3 s + b_3}{1 + s^2/(3 \times 2\pi f_x)^2}, \tag{22}$$

where, K_i denotes for the integral gain, f_x [Hz] is the fundamental frequency of the input reference, $\omega_k = k \cdot 2\pi f_x$ with $k \in \{1,2,3\}$ are the natural frequencies of the components of IMC respectively, a_k and b_k with $k \in \{1,2,3\}$ are the parameters chosen by the user for a proper IMC controller. Usually, these parameters can be determined using an affine parameterization approach in [18, 21] or a trial and error approach based on the user's experience as adopted in [24].

Remark 2: We here suggest that the two aforementioned approaches for parameters' determination in an IMC scheme can be merged in practice. To be more specific, the affine parameterization approach aims to design proper parameters such that the closed-loop poles locate in desired positions by solving a closed-loop characteristic polynomial [18]. Therefore, it can be utilized firstly to choose an initial set of parameters while maintain the stability of the closed-loop. However, the obtained IMC may be a high-order controller so that it is hard to be implemented. For this, an order reduction can be operated using a balanced realization. Then, a trial and error approach can be applied to tune the parameters slightly to obtain acceptable rejection or tracking of the corresponding exogenous signals [24]. By merging the two methods in design, both stability and performance can be satisfied. This is utilized in the subsequent controller design in this work.

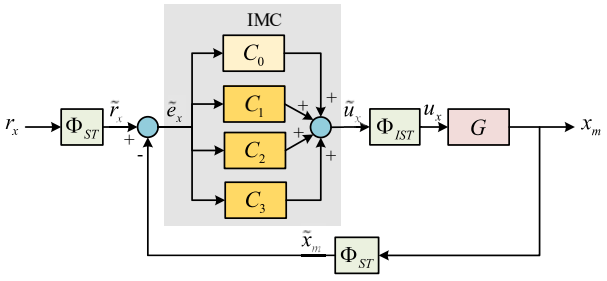

Fig. 4. The proposed STIMC scheme.

3.3. Stability and performance analysis

In the proposed STIMC scheme, before driving the nanopositioning stage, an inverse transformation $\Phi_{IST}(s)$ of the generated control signals are operated . Also, in the feedback loop, a signal transformation $\Phi_{ST}(s)$ is added for the calculation of transformed errors $\widetilde{e}_x$.

In Fig. 4, the closed-loop transfer function from input r_x to measured output x_m of the proposed STIMC can be obtained as

$$\begin{aligned} T(s) &= \frac{x_m(s)}{r_x(s)} \\ &= \Phi_{ST}(s) \cdot \frac{C_{IMC}(s) \cdot \Phi_{IST}(s) \cdot G(s)}{1 + C_{IMC}(s) \cdot \Phi_{IST}(s) \cdot G(s) \cdot \Phi_{ST}(s)} \\ &= \frac{C_{IMC}(s) \cdot G(s)}{1 + C_{IMC}(s) \cdot G(s)}, \end{aligned} \tag{23}$$

where $C_{IMC} = \sum_{i=0}^{3} C_i$ is the designed IMC, the transformation operator and the inverse transformation operator satisfy $\Phi_{ST}(s) \cdot \Phi_{IST}(s) = 1$. Equation (23) implies that the introduction of the signal transformation in STIMC has no effect on the stability of the closed-loop providing that $\Phi_{ST}(s) \neq 0$ and $\Phi_{IST}(s) \neq 0$ for all frequencies.

Hereto, the internal stability condition of the closed-loop with STIMC is equivalent to the closed-loop with IMC. According to the internal stability condition in [25].

The sensitivity transfer function from the input r_x to the tracking error $\widetilde{e}_x$ of the proposed STIMC can be derived as

$$\begin{aligned} S(s) &= \frac{\widetilde{e}_x(s)}{r_x(s)} \\ &= \frac{\Phi_{ST}(s)}{1 + C_{IMC}(s) \cdot G(s)}. \end{aligned} \tag{24}$$

Note that $\widetilde{r}_x(s) = \Phi_{ST}(s) \cdot r_x(s)$, therefore we denote transformed sensitivity transfer function as the dynamics from the transformed input $\widetilde{r}_x$ to the tracking error $\widetilde{e}_x$:

$$\widetilde{S}(s) \triangleq \frac{\widetilde{e}_x(s)}{\widetilde{r}_x(s)}$$

$$= \frac{1}{1 + C_{IMC}(s) \cdot G(s)} = \frac{D_c \cdot D_G}{D_C \cdot D_G + N_C \cdot N_G}, \quad (25)$$

where $C_{IMC} \triangleq N_C/D_C$, and $G \triangleq N_G/D_G$ with N_C, N_G standing for the numerators of C_{IMC} and G while D_C, D_G denoting the denominators.

Recall the functions of IMC in (19)-(22), the numerator of $\widetilde{S}(s)$ can be derived as

$$N_{\widetilde{S}}(s) = D_C \cdot D_G = s \cdot \prod_{k=1}^{3}(s^2 + \omega_k^2) \cdot D_G. \quad (26)$$

Substitute $s = j\omega$ into (26), the frequence response of $N_{\widetilde{S}}$ can be obtained as,

$$N_{\widetilde{S}}(j\omega) = j\omega \cdot \prod_{k=1}^{3}(\omega^2 - \omega_k^2) \cdot D_G(j\omega), \quad (27)$$

where $\omega = 2\pi f_x$ is the input reference's frequency.

Note that the natural frequencies of IMC components (i.e., ω_k) are set as $k \cdot 2\pi f_x$. Therefore, following results can be expected from (27) as:

- If the input reference only contains the fundamental frequency f_x, then $N_{\widetilde{S}}(j\omega) = 0$, which implies that the tracking error will be 0 under the control of C_1 without consideration of exogenous disturbance and noise.
- If the input reference contains the basic frequency f_x as well as its frequency doubling in second-order and/or even third-order, then $N_{\widetilde{S}}(j\omega) = 0$ will also remain, which implies that the exogenous disturbances or noises which are two and/or three times of the fundamental frequency will be attenuated dramatically because of the introduction of C_1 , C_2 and/or C_3.
- For exogenous disturbances or noises in other frequencies, $N_{\widetilde{S}}(j\omega) \neq 0$. However, as the existence of C_0, the closed-loop dynamics with STIMC will be a type-1 system (i.e., a balanced system with one integral), which means that errors resulted from these frequencies will also be rejected gradually and markedly by choosing a proper gain K_i.

Remark 3: As is well known, steady tracking error of a slope signal for a type-1 system is proportional to its slope ratio. In an IMC scheme, a Cycloid or Spiral signal will not be perfectly tracked as they both contain slope components. Fortunately, by applying the transformation of Φ_{ST}, the slope components in a Cycloid signal as in (10) or a Spiral signal as in (14) will be removed. For this, for the closed-loop dynamics with a type-1 system, the STIMC scheme is expected to obtain a further improvement for reference's tracking when compared with the IMC scheme.

3.4. Overall design procedure

Hereto, the overall design procedure for the proposed STIMC can be summarized as below.

Step 1: Identify the nominal model of the nanopositioning system as shown in Fig. 2.

Step 2: Design the transformation and the inverse transformation operators for the given non-raster scanning references. Refer to Section 3.1 for specific examples.

Step 3: Determine the integral controller C_0 for stable convergence of the tracking error.

Step 4: Tune the parameters in C_1, C_2 and C_3 for improved tracking precision through simulations as described in Remark 2.

Step 5: Adjust the parameters in C_2 and C_3 to further alleviate the residual errors resulted from the nonlinearity of hysteresis through experiments.

Step 6: Stop.

Remark 4: In this procedure, for the precise tracking of a harmonic waveform with fixed frequency, the parameters in C_2 and C_3 can be chosen preliminarily through simulations and determined finally through experiments. Therefore, the hysteresis modelling work is not necessary.

4. CONTROLLER IMPLEMENTATION

In this section, the effectiveness of the proposed STIMC scheme is verified through conducting a series of experiments on the nanopositioning stage displayed in Fig. 1. Two set of the three non-raster scanning patterns at 25 Hz and 50 Hz are tested for comparisons of STIMC and conventional IMC. To make fair comparisons, the parameters of the internal models in the STIMC are chosen the same as the conventional IMC in the experiments.

4.1. Controller design

4.1.1 C_0

The integral feedback tracking controller can be determined using a graphical method as reported in [26]. The basic idea is to tune the controller gain such that the required stability region condition can be satisfied. Here, the controller gain is designed as $k_i = 100$.

4.1.2 C_1, C_2, C_3

For the design of the first order internal model, a H_∞ mixed-sensitivity synthesis method [21] is adopted for the pole placement such that robust loopshaping of C_1. The weighting function for loop sensitivity is designed as,

$$W_1(s) = \frac{1}{1 + 10^{-4}s/(2\pi f) + s^2/(2\pi f)^2}, \quad (28)$$

where f [Hz] is the reference's frequency, a term $10^{-4}s/(2\pi f)$ is contained for the stability of W_1 in computation, the poles at $2\pi f$ are induced by C_1. A weighting function

Table 1. Controller parameters for harmonic signal tracking at 25 and 50 Hz.

		$C_1(\times 10^{-4})$		$C_2(\times 10^{-4})$		$C_3(\times 10^{-4})$	
		a_1	b_1	a_2	b_2	a_3	b_3
25Hz	Liss.	-1430	50	100	10	10	1
	Cyc.	-2210	40	1	0.01	1	0.01
	Spi.	-920	30	10	0.01	1	0.01
50Hz	Liss.	-1840	8.15	100	0.5	10	0.5
	Cyc.	-2390	5.85	1	0.02	2	0.04
	Spi.	-1200	5.48	1	0.01	1	0.01

for control gain is designed as,

$$W_2(s) = 5. \tag{29}$$

Hereto, a minimization process is operated using the command of *mixsyn* in Matlab environment. A second order controller of C_1 is then can be obtained after a model reduction of the synthesized high order controller.

Finally, the parameters in C_2 and C_3 are tuned through experiments to achieve acceptable tracking precision as described in [24]. Here, the designed results of the controllers for 25 Hz and 50 Hz harmonic waveforms are given respectively in Table 1.

4.2. Experimental results

A set of experiments were implemented to evaluate the performance of the designed IMC and STIMC controllers. Tracking results are displayed in Figs. 5-10 with the statistical root-mean-square (RMS) errors listed in Table 2. The three scanning patterns are discussed step by step in the following parts. The effects of STIMC will be observed gradually through comparisons with IMC.

4.2.1 Lissajous scanning

Figs. 5 and 6 show the experimental tracking results of 25 Hz and 50 Hz Lissajous scanning pattern. As indicated in (8) and (9), the signal transformation and the inverse transformation operators are simple constants. For this, the proposed STIMC is predicted to perform as well as the conventional IMC providing that parameters of the internal modes are the same. Experimental results verified this

Table 2. Statistical Results of RMS Errors of Non-raster Scanning Tracking at 25 and 50 Hz.

eRMS (μm)		25 Hz		50 Hz	
		x-axis	y-axis	x-axis	y-axis
Liss.	IMC	0.384	0.384	0.544	0.557
	STIMC	0.383	0.385	0.556	0.550
Cyc.	IMC	0.264	0.127	0.263	0.128
	STIMC	0.129	0.126	0.123	0.128
Spi.	IMC	0.113	0.109	0.122	0.117
	STIMC	0.012	0.015	0.024	0.019

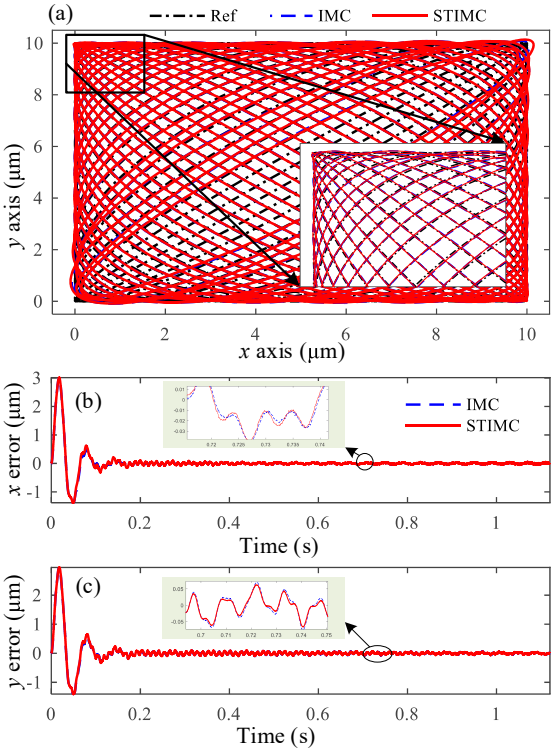

Fig. 5. Tracking results of 25 Hz Lissajous scanning pattern: (a) Overall view; (b) and (c) Tracking errors.

point as we can see both the x and y axes tracking errors under STIMC are close to those under IMC. Herein, for this case, the signal transformations result in no improvements on the closed-loop tracking performance. However, on the other hand, it also demonstrates directly that the transformations have no effects on the internal stability of the closed-loop, which is consistent with (23).

Moreover, tracking performance trends to be a bit worse for 50 Hz, which involves much high-frequency errors in the steady stage as shown in Fig. 6(b) and (c). To be more specific, an RMS error of 0.544 μm is obtained for x-axis at 50 Hz, which is a 42% increase from 0.384 μm at 25 Hz. Similar results can be observed in view of the y-axis. The main reason for this is the undesired vibrations caused by the lightly-damped resonant modes in this system. A well-designed damping controller can be adopted for the performance improvements [27, 28]. It should be noted that combing damping controller with STIMC is not the main object for this work, therefore, the experiments of such composite controller were not included for brief.

4.2.2 Cycloid scanning

Experimental results of the cycloid scanning pattern are displayed in Figs. 7 and 8. In this pattern, the signal transformation and the inverse transformation operators for y-axis are simple constants, while the operators for x-axis

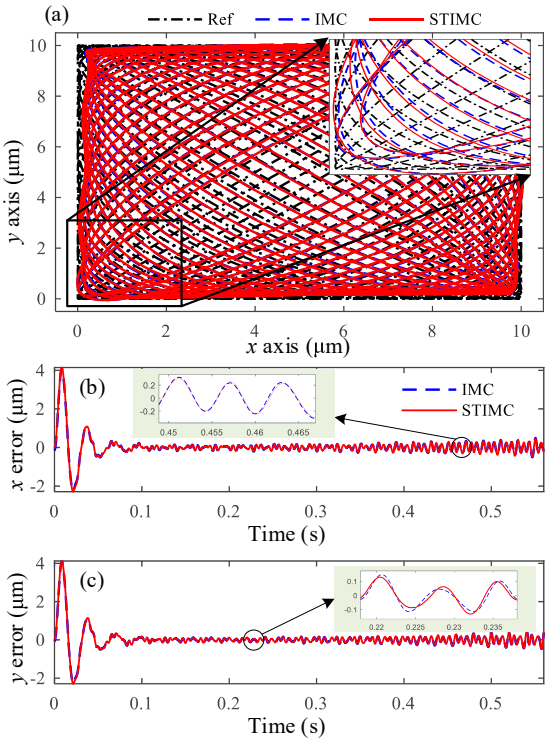

Fig. 6. Tracking results of 50 Hz Lissajous scanning pattern: (a) Overall tracking view; (b) and (c) Tracking errors of x and y axes.

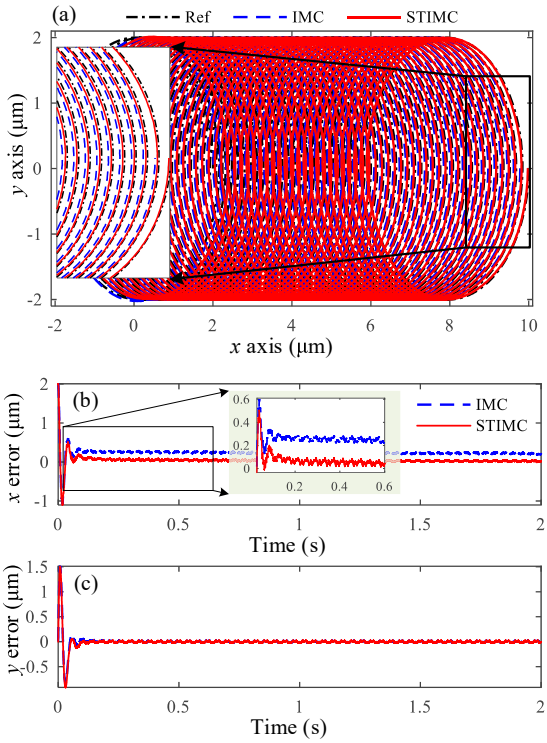

Fig. 7. Tracking results of 25 Hz cycloid scanning pattern: (a) Overall tracking view; (b) and (c) Tracking errors of x and y axes.

are effective.

As analyzed in Remark 3, the slope component in the x-axis of a Cycloid signal is removed by the transformation operator in the STIMC scheme, therefore, improvements can be achieved for the x-axis tracking, which are 51% and 53% in the RMS errors from IMC to STIMC at 25 and 50 Hz as illustrated in Fig. 7(b) and Fig. 8(b), respectively.

4.2.3 Spiral scanning

In this pattern, both the two axes are transformed by time-varying operators. The ever-increasing amplitudes should have a direct impact on the tracking accuracy with increasing errors under conventional IMC control. After transformation to constant amplitudes by STIMC, the time-varying amplitudes are modified, and the tracking performances for both the two axes are predicted to be improved distinctly. Results in Figs. 9 and 10 have demonstrated this. The overall tracking errors for STIMC are smaller and steadier than those under IMC.

To be specific, in the 25 Hz case, the RMS errors of x-axis is decreased dramatically from 0.113 μm with IMC to 0.012 μm with STIMC, which is an 89% promotion of accuracy. For y-axis, such improvement is 86%. Similar results can be obtained in the 50 Hz case. Tracking accuracy is promoted by 80% for x-axis and 83% for y-axis, respectively.

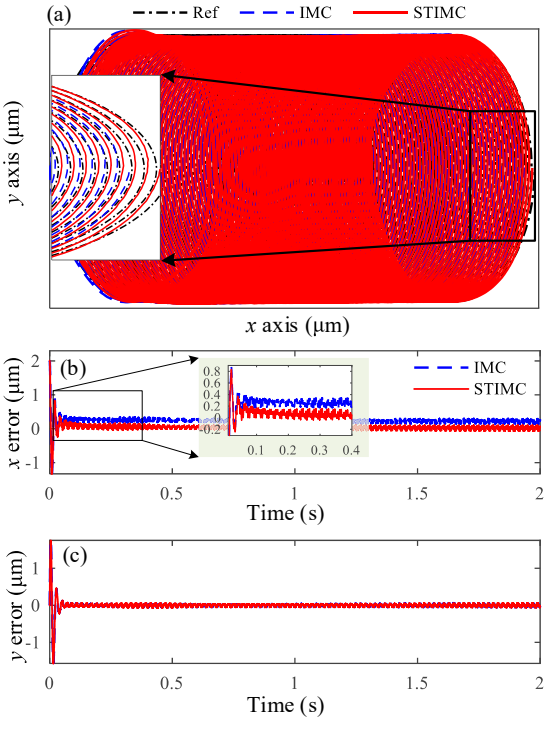

Fig. 8. Tracking results of 50 Hz cycloid scanning pattern: (a) Overall view; (b) and (c) Tracking errors.

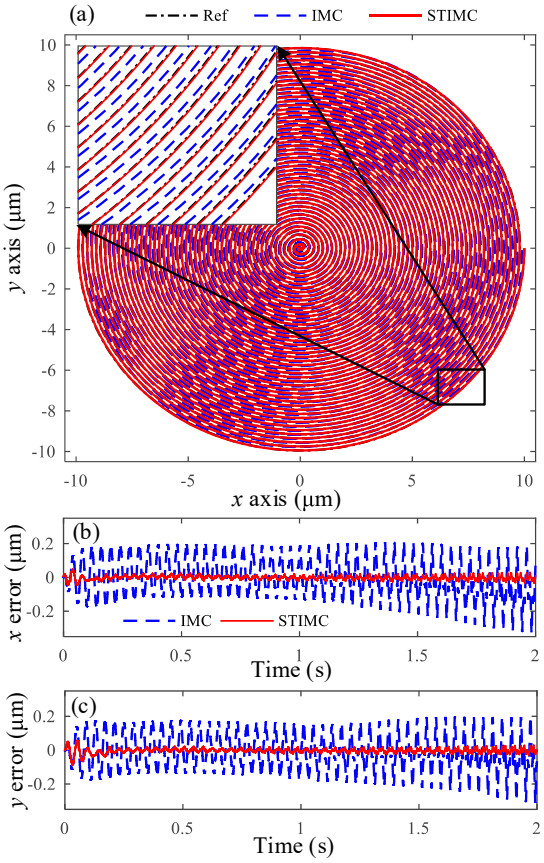

Fig. 9. Tracking results of 25 Hz spiral scanning pattern: (a) Overall view; (b) and (c) Tracking errors.

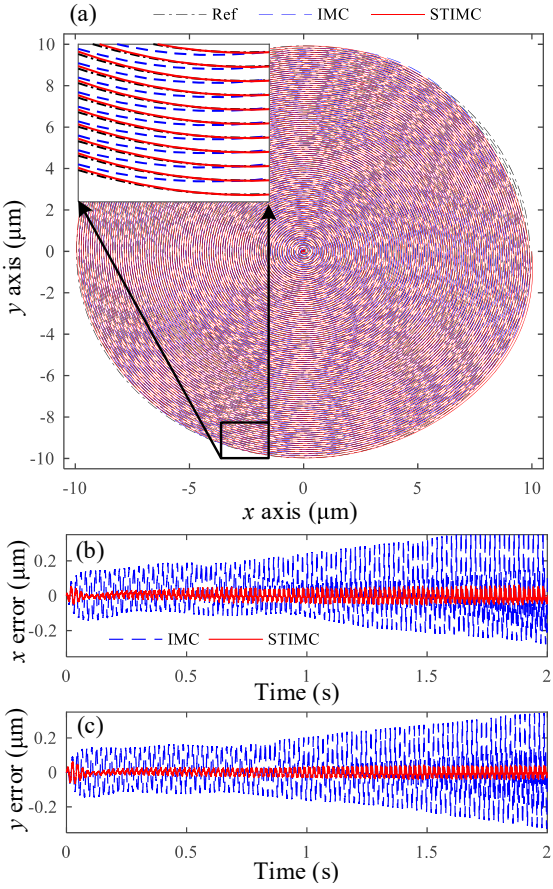

Fig. 10. Tracking results of 50 Hz spiral scanning pattern: (a) Overall view; (b) and (c) Tracking errors.

5. CONCLUSION

In this work, a signal transformed internal model control (STIMC) approach was presented for precise tracking of non-raster scanning patterns for piezo nanopositioning stage. For the design of STIMC, signal transformation and inverse transformation operators were calculated for converting the references into standard harmonic signals with fixed frequency and constant amplitude. A set of internal modes were then designed for accuracy improvements. The first order internal mode was determined through H_∞ approach, and the second as well as the third controller parameters were tuned through experiments. Experimental results demonstrated the effectiveness and superiority of the proposed STIMC over conventional IMC. A same tracking precision for Lissajous scanning could be obtained by STIMC compared with IMC. The tracking accuracy improvement was obtained by larger than 50% for cycloid scanning pattern, and a decrease 80% of tracking errors over was achieved for spiral scanning pattern.

Future work will seek to enhance the tracking performance of these non-raster scanning patterns by integrating damping control with IMC. Besides, the disturbance and noise rejection need to be considered in the SPM scanning applications.

REFERENCES

[1] M. S. Rana, H. R. Pota, and I. R. Petersen, "Improvement in the imaging performance of atomic force microscopy: a survey," *IEEE Transactions on Automation Science and Engineering*, vol. 14, no. 2, pp. 1265-1285, Apr. 2017.

[2] J. Ling, M. Rakotondrabe, Z. Feng, M. Ming, and X. Xiao, "A robust resonant controller for high-speed scanning of nanopositioners: design and implementation," *IEEE Transactions on Control Systems Technology*, 2019. DOI: 10.1109/TCST.2019.2899566

[3] T. Tuma, A. Sebastian, J. Lygeros, and A. Pantazi, "The four pillars of nanopositioning for scanning probe microscopy: The position sensor, the scanning device, the feedback controller, and the reference trajectory," *IEEE Control Systems Magazine*, vol. 33, no. 6, pp. 68-85, Dec. 2013.

[4] Y. F. Shan and K. K. Leang, "Design and control for high-speed nanopositioning: serial-kinematic nanopositioners and repetitive control for nanofabrication," *IEEE Control Systems Magazine* , vol. 33, no. 6, pp. 86-105, Dec. 2013.

[5] J. Ling, Z. Feng, M. Ming, and X. Xiao, "Model reference adaptive damping control for a nanopositioning stage with load uncertainties," *Review of Scientific Instruments*, vol. 90, no. 4, pp. 045101, Apr. 2019.

[6] Y. R. Teo, Y. Yong, and A. J. Fleming, "A comparison of scanning methods and the vertical control implications for scanning probe microscopy," *Asian Journal of Control*, vol. 19, no. 2, pp. 1352-1366, Jul. 2018.

[7] A. A. Eielsen, M. Vagia, J. T. Gravdahl, and K. Y. Pettersen, "Damping and tracking control schemes for nanopositioning," *IEEE/ASME Transactions on Mechatronics*, vol. 19, no. 2, pp. 432-444, Apr. 2014.

[8] C. X. Li, Y. Ding, G. Y. Gu, and L. M. Zhu, "Damping control of piezo-actuated nanopositioning stages with recursive delayed position feedback," *IEEE/ASME Transactions on Mechatronics*, vol. 22, no. 2, pp. 855-864, Apr. 2017.

[9] K. K. Leang and B. J. Kenton, "Design and control of a three-axis serial-kinematic high-bandwidth nanopositioner," *IEEE/ASME Transactions on Mechatronics*, vol. 17, no. 2, pp. 356-369, Apr. 2012.

[10] Z. Feng, J. Ling, M. Ming, and X. Xiao, "Integrated modified repetitive control with disturbance observer of piezoelectric nanopositioning stages for high-speed and precision motion," *Journal of Dynamic Systems Measurement and Control*, vol. 141, no. 8, pp. 081006, Mar. 2019.

[11] Z. Wu and Q. Xu, "Survey on recent designs of compliant micro-/nano-positioning stages," *Actuators*, vol. 7, no. 1, pp. 5, Feb. 2018.

[12] M. Ming, J. Ling, Z. Feng, and X. Xiao, "A model prediction control design for inverse multiplicative structure based feedforward hysteresis compensation of a piezo nanopositioning stage," *International Journal of Precision Engineering and Manufacturing*, vol. 19, no. 11, pp. 1699-1708, Nov. 2018.

[13] D. Habineza, M. Zouari, Y. Gorrec, and M. Rakotondrabe, "Multivariable compensation of hysteresis, creep, badly damped vibration, and cross couplings in multiaxes piezoelectric actuators," *IEEE Transactions on Automation Science and Engineering*, vol. 15, no. 4, pp. 1639-1653, Oct. 2018.

[14] Q. Xu, "Precision motion control of piezoelectric nanopositioning stage with chattering-free adaptive sliding mode control," *IEEE Transactions on Automation Science and Engineering*, vol. 14, no. 1, pp. 238-248, Jan. 2017.

[15] M. Hammouche, P. Lutz, and M. Rakotondrabe, "Robust and optimal output-feedback control for interval state-space model: application to a two-degrees-of-freedom piezoelectric tube actuator," *Journal of Dynamic Systems, Measurement, and Control*, vol. 141, no. 2, pp. 021008, Oct. 2018.

[16] Y. K. Yong, A. Bazaei, and S. O. R. Moheimani, "Video-rate Lissajous-scan atomic force microscopy," *IEEE Transactions on Nanotechnology*, vol. 13, no. 1, pp. 85-93, Jan. 2014.

[17] N. Nikooienejad, A. Alipour, M. Marou, and S. O. R. Moheimani, "Sequential cycloid scanning for time-resolved atomic force microscopy," *Proc. of the 2018 IEEE/ASME International Conference on Advanced Intelligent Mechatronics*, pp. 125-130, 2018.

[18] A. Bazaei, M. Marou, A. G. Fowler, and S. O. R. Moheimani, "Internal model control for spiral trajectory tracking With MEMS AFM scanners," *IEEE Transactions on Control Systems Technology*, vol. 24, no. 5, pp. 1717-1728, Sep. 2016.

[19] A. Bazaei, M. Marou, and S. O. R. Moheimani, "Tracking of constant-linear-velocity spiral trajectories by approximate internal model control," *Proc. of the 2017 IEEE Conference on Control Technology and Applications*, pp. 27-30, 2017.

[20] A. Bazaei, Y. K. Yong, and S. O. R. Moheimani, "High-speed Lissajous-scan atomic force microscopy: Scan pattern planning and control design issues," *Review of Scientific Instruments*, vol. 83, no. 6, pp. 063701, Jun. 2012.

[21] A. Bazaei, Y. K. Yong, and S. O. R. Moheimani, "Combining spiral scanning and internal model control for sequential AFM imaging at video rate," *IEEE/ASME Transactions on Mechatronics*, vol. 22, no. 1, pp. 371-380, Jun. 2016.

[22] I. A. Mahmood, S. O. R. Moheimani, and B. Bhikkaji, "A new scanning method for fast atomic force microscopy," *IEEE Transactions on Nanotechnology*, vol. 10, no. 2, pp. 203-216, Mar. 2011.

[23] M. Rakotondrabe, "Multivariable classical Prandtl–Ishlinskii hysteresis modeling and compensation and sensorless control of a nonlinear 2-dof piezoactuator," *Nonlinear Dynamics*, vol. 89, no. 1, pp. 481-499, Jul. 2017.

[24] A. Alipour, N. Nikooienejad, M. Maroufi, and S. O. R. Moheimani, "Internal model control of cycloid trajectory for video-rate AFM imaging with a SOI-MEMS nanopositioner," *Proc. of the American Control Conference*, pp. 2916-2921, Jun. 2018.

[25] J. C. Doyle, B. A. Francis, and A. R. Tannenbaum, *Feedback Control Theory*, ch. 3, sec. 2, pp. 31-32, Courier Corporation, North Chelmsford, USA, 2013.

[26] L. L. Li, C. X. Li, G. Y. Gu, and L. M. Zhu, "Positive acceleration, velocity and position feedback based damping control approach for piezo-actuated nanopositioning stages," *Mechatronics*, vol. 47, pp. 97-104, Nov. 2017.

[27] J. Ling, Z. Feng, M. Ming, and X. H. Xiao, "Damping controller design for nanopositioners: A hybrid reference model matching and virtual reference feedback tuning approach," *International Journal of Precision Engineering and Manufacturing*, vol. 19, no. 1, pp. 13-22, Jan. 2018.

[28] Z. Feng, J. Ling, M. Ming, and X. H. Xiao, "High-bandwidth and flexible tracking control for precision motion with application to a piezo nanopositioner," *Review of Scientific Instruments*, vol. 88, no. 8, pp. 085107, Jul. 2017.

Jie Ling received his B.S. and Ph.D. degrees in Mechanical Engineering from School of Power and Mechanical Engineering, Wuhan University, China, in 2012 and 2018, respectively. He was a joint Ph.D. student with Department of Automatic Control and Micro-Mechatronic Systems, FEMTO-st Institute, France in 2017. From 2019 to 2020, he is a joint Postdoc Researcher with Department of Biomedical Engineering, National University of Singapore, Singapore. Since 2018, he has been a Postdoctoral Researcher with Department of Mechanical Engineering, Wuhan University, Wuhan, China. His research interests include mechanical design and precision motion control of nanopositioning stages and micromanipulation robots.

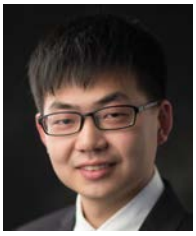

Zhao Feng received his B.S. degree in Mechanical Engineering from School of Power and Mechanical Engineering, Wuhan University, Wuhan, China in 2010. He is currently pursuing a Ph.D. degree in Mechanical Engineering at Wuhan University, Wuhan, China. He is now a joint Ph.D. student at the Department of Electrical and Computer Engineering, National University of Singapore. His research interests include vibration control, iterative learning control, nanopositioning and robotics.

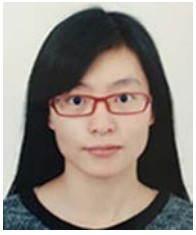

Min Ming received her B.S. degree in Mechanical Engineering from Wuhan, China in 2014. She is currently pursuing a Ph.D. degree in Mechanical Engineering at Wuhan University, Wuhan, China. Her research interest covers hysteresis compensation, iterative learning control, and nanopositioner.

Zhao Guo received his B.S. and M.S. degrees in Mechanical Engineering from Jiangsu University, China, in 2004 and 2007, respectively, and his Ph.D. degree in Mechatronics Engineering from Shanghai Jiao Tong University, China, in 2012. From 2012 to 2015, He was a Research Fellow with the Department of Biomedical Engineering, National University of Singapore (NUS), Singapore. Dr. Guo is currently an Associate Professor with School of Power and Mechanical Engineering, Wuhan University, China. His research interests include compliant actuator, exoskeleton design, modeling and control, and physical human robot interaction. He mainly focuses on the area of rehabilitation robotics.

Xiaohui Xiao received her B.S. and M.S. degrees in Mechanical Engineering from Wuhan University, Wuhan, China, in 1991 and 1998, respectively, and a Ph.D. degree in mechanical engineering from Huazhong University of Science and Technology, Wuhan, China, in 2005. From 2006 to 2008, she was a Research Fellow with the Department of Mechanical Science and Engineering, University of Illinois at Urbana-Champaign, USA. She joined Wuhan University,Wuhan, China, in 1998, where she is currently a Full Professor with the Mechanical Engineering Department, School of Power and Mechanical Engineering. Dr. Xiao has published a number of papers in the areas of mobile robots, dynamics and control, sensors and signal procession. Her current research interests include mobile robotics, high-precision positioning control, and signal processing.